RESULTS OF A SPACE DOSIMETRY EXPERIMENT TO ASSESS RADIATION PROTECTION CALCULATIONS FOR MANNED SPACE FLIGHT

M. C. CHAPMAN* and R. E. FORTNEY
Northrop Space Laboratories, Hawthorne, California, U.S.A.

and

F. E. HOLLY and R. STOVALL
Air Force Weapons Laboratory, Kirtland AFB, New Mexico, U.S.A.

Abstract—On October 5,1965, a dosimetry satellite was placed in a rectrograde earth orbit with an inclination of 144°. Apogee and perigee were 3460 km and 411 km respectively. This orbit was such that virtually all of the inner Van Allen zone was covered. The instrumentation package consisted of seven separate electron and proton spectrometers (0.56 to 5 MeV for electrons—10 to 120 MeV for protons), a proton depth-dosimeter measuring absorbed energy at three depths in an aluminum shield, an X-ray or bremsstrahlung spectrometer measuring secondary dose behind an aluminum shield, and two tissue equivalent ionization chambers. Thus proton and electron tissue dose and bremsstrahlung production were measured simultaneously with both uni- and omni-directional radiation environment data. The material distribution of the satellite was experimentally determined and a magnetometer was used to relate spacecraft geometry to particle distributions in space. Therefore, a controlled experiment was performed to investigate the importance of simplifying assumptions in the calculation of proton and electron doses as well as a measurement of the spatial dose and particle distributions. Utilizing this data, representative doses are calculated and compared with the results of the on-board dosimetry.

I. INTRODUCTION

With the advent of manned space flight it became apparent that space radiations would play a significant role in man's ability to successfully negotiate space. Radiations trapped in the magnetosphere (Van Allen Regions), Galactic Cosmic Rays, and Solar Flare Radiation could presumably limit the duration of any space mission.[1]

Many computer programs have been developed which use various theoretical models of the space radiation environment. Ideally, when all relevant factors are known to a high degree of precision, only a single computer program will be required. Such a program would require only two inputs—the shielding configuration of the vehicle and its proposed spatial path; the radiation environment being contained within the program. Programs such as this have been developed for the Air Force by the Boeing Corporation[2] and Northrop Space Laboratories[3] and are represented by the flow chart in Fig. 1. In any program where information is accumulated step by step, the error in the end result is cumulative. Therefore, the accuracy of the end result can be no better than the accuracy of a single input or step, and each of the eight inputs or blocks of Fig. 1 must be known to a high degree of precision. Extensive experimental programs are under way to test the ability of these computer programs to predict dosages received by space-crew members during an arbitrary space mission. It is the purpose of this paper to describe one such experiment which has been performed.

Assuming that dose can be measured in biologically relevant terms, one experiment would

* Now at TRW Systems Laboratories, Redondo Beach, California, USA.

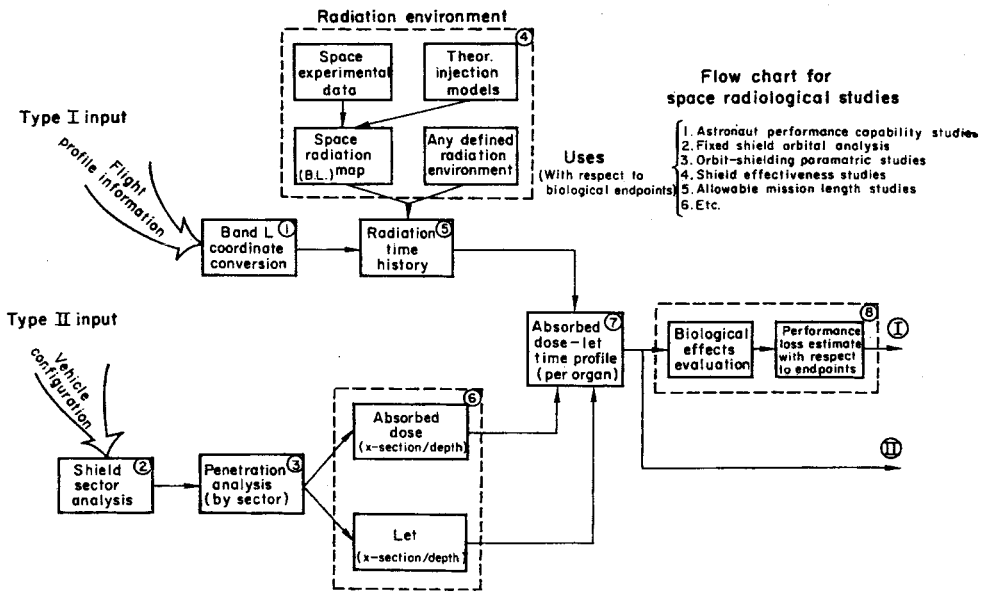

FIG. 1. Flow chart for space radiological studies.

be simply to measure the dose at some arbitrary spatial location and compare this measurement with calculated results. This implies a strong reliance on previously gathered environmental data (Block 4, Fig. 1). Since the environment may change slowly with time and rapidly with spatial position, difficulties may arise in comparing a computed dose for a point or points in space with an actual measurement. The experiment described herein obviates the necessity for reliance on past environmental data by adopting the philosophy of simultaneous measurement of the radiation environment and absorbed dosage. This allows the following goals to be accomplished:

1. Provide extra measurements of the radiation environment for further updating of the computer program.
2. Provide measurements of absorbed dosages throughout space.
3. Provide valid checks on the shielding analysis, radiation transport, and dosage computation portions of the computer program by elimination of the environmental portion of the program.

II. EXPERIMENTAL TECHNIQUE

A. *Instrumentation*

Our experiment was designed with a single philosophical ground-rule—that of providing simultaneous measurement of the radiation environment and absorbed dose in such a manner that the results may be used to check theoretical calculations.

To this end, a satellite was instrumented with seven separate electron and proton spectrometers for the complete measurement of the entire radiation environment and four instruments to measure absorbed dosage. Brief descriptions of these instruments are contained in Tables 1 and 2.

The flux, energy spectra, and angular distributions of electrons and protons were measured by four directional spectrometers employing scintillation techniques and multichannel analyzers. Three instruments, provided by Aerospace Corporation, measured the omnidirectional flux and energy spectra of electrons and protons and employed solid state ionization techniques.[4] The above instruments utilize well-known techniques and will not be described in further detail. They provided measurements of the radiation environment over the energy ranges of 0.56 to 5 MeV for electrons and 6 to 160 MeV for protons. These instruments were well calibrated utilizing Sr^{90} and Cs^{137} beta sources and the 50 MeV proton accelerator facility at the University of California at Los Angeles.

For the measurement of absorbed dose, four

Table 1. Environmental Instrumentation

Instrument	Number used	Detector	Type of measurement	Dynamic range
Electron spectrometer	1	CsI—plastic phoswich with pulse height analysis	Electron flux energy spectra, angular distribution	0.5 to 10^4 counts/sec. 0.5 to 5.0 MeV in eight channels
Proton spectrometer	1	Same as above with plastic absorber	Proton flux, energy spectrum, angular distribution	0.5 to 10^3 counts/sec. 49 to 120 MeV in four channels
Delta E proton spectrometers	2	Thin plastic scintillators with threshold detection	Integral proton flux between limits, angular distribution	Delta E_1: 5×10^{-1} to 5×10^2 counts/sec. (10 MeV $< E <$ 20 MeV) Delta E_2: 5×10^{-1} to 5×10^2 counts/sec. (20 MeV $< E <$ 49 MeV)
Omni-directional* proton-electron spectrometers	3	Solid state detector with threshold	Integral proton flux between limits	Protons: 6–20, 40–80, 100–160, and < 100 MeV
			Integral electron flux above threshold	Electrons: 0.3 and 4.5 MeV

* Provided by Aerospace Corporation, El Segundo, California.

Table 2. Dosimetric Instrumentation

Instrument	Number used	Detector	Type of measurement	Dynamic range
Proton dosimeter	1	Solid state detectors imbedded in Al sphere at depths of 0, 4, and 16 g/cm^2	Energy deposition at known depths in simple geometry	0.5 to 2×10^4 MeV/sec (each detector)
X-ray or bremsstrahlung dosimeter	1	Thin CsI crystal behind known aluminum shield	Energy deposition per unit time caused by bremsstrahlung from electrons striking known shield	1.62×10^3 to 1.62×10^6 MeV/sec.
Tissue-equivalent	2	Small ionization chamber constructed of Shonka Muscle-equivalent plastic	Absorbed dose in rad/hr at depth of 0.17., 3.2 and 8 g/cm^2	0.2 to 200 rad/hr

instruments of three types were utilized. They are as follows:

1. Tissue Equivalent Ionization Chambers (T.E.I.C.). Two instruments of this type were utilized and imbedded in a tissue-equivalent material (lucite) at depths of 0.17 and 3.2 g/cm^2. Anisotrophy of shielding provided another apparent depth of 8.0 g/cm^2 in certain instances. Basically these chambers are constructed of Shonka muscle-equivalent plastic and are described in the literature in numerous places.[5, 6] A thorough calibration was performed utilizing Sr^{90} and Cs^{137} beta sources as well as the proton accelerator facilities at Oak Ridge National Laboratory and Harvard University.

2. Proton Dosimeter Sphere. The proton dosimeter is designed to measure, primarily, proton dose rates penetrating various degrees of shielding material in a simple geometry. This measurement is achieved by using solid state detectors placed at three different depths in an aluminum sphere: 0, 4 and 16 g/cm^2. To obtain a wide dynamic range with good accuracy, the instrument alternates between two overlapping sensitivity ranges. The solid state detectors produce a signal proportional to the energy deposited by an intercepted proton in the semiconductor material. This signal is amplified by a charge-sensitive solid state preamplifier and fed to a pulse height discriminator which rejects noise and signals below a predetermined level. The pulse-height discriminator passes signals above this level to the pulse-height to pulse-width converter, where each pulse is converted to a constant amplitude pulse whose width is proportional to its height. These pulses are then fed to a log-integrator which integrates the signal for a variable-known time. The sensitivity of the proton dosimeter is controlled by alternately increasing and decreasing the integrating period.

The three solid state detectors were calibrated so that the output in volts may be related directly to rate of energy deposition in the detectors. The parameters which had to be determined included detector sensitive area and thickness and the relation between detector pulse height and energy deposited.

The Ph/PW converters for all three channels have a nominal 20 μsec/V conversion factor. To establish accurately the integrating time versus particle energy, the gain is adjusted using a radioactive calibration source to obtain pulse widths corresponding to each channel's sensitivity. A monoenergetic 5.30 MeV alpha source and Cs^{137} and Sr^{90} beta sources were used as calibration sources to accurately adjust gains and to establish the acceptance threshold level of the pulse height discriminator at 0.5 MeV.

Having set the gains of the preamps and electronic thresholds, it was desirable to calibrate the system at various dose rates, simulating as closely as possible the nuclear environment (random rates and pulse heights). It was possible to approximate this condition by generating a random pulse-rate of constant amplitude pulses that closely simulated the pulse shape from the detectors. The rate and amplitude were varied and recorded, along with the dosimeter output.

In addition to the calibration of the various electronic assemblies mentioned previously, four of the solid-state detectors were calibrated at the University of Southern California 30 MeV Proton Accelerator. Calibration consisted of a set of identical experiments to determine detector thickness for all four detectors.

Energy loss in the detector (which is proportional to the pulse-height output from the charge sensitive preamplifier) is a linear function of the energy of the incident particle as long as this energy is sufficiently low that it is completely absorbed in the detector. If all energy is not absorbed in the detector, the energy loss in the detector decreases as the incident energy increases. The thickness corresponding to total absorption may be uniquely determined.

The final calibration of each detector within the system consisted of placing the dosimeter in a flight configuration and exposing each detector to Sr^{90} beta particles. The output (in volts) of the dosimeter was noted, and the output analyzed. The data collected from the multichannel analyzer can be integrated to yield the MeV/sec exceeding the known (0.5 MeV) threshold and this measured total dose compared with the dosimeter output. The agreement among measurements using this technique was found to be excellent.

3. X-Ray Bremsstrahlung Dosimeter. The X-ray dosimeter is designed to measure the energy per unit time which bremsstrahlun

from electrons striking a known shielding will produce in a thin CsI crystal. This allows the assessment of results of calculations of bremsstrahlung within shielding media. The sensor consists of a small CsI crystal (0.25 in. in diameter by 0.020 in. thick) cemented to a photomultiplier tube. The output current from the anode of the photomultiplier tube is converted into a voltage which is proportional to the logarithm of the current.

Calibration of this instrument was accomplished in the following manner. The energy flux striking the CsI crystal was calculated for peak flux in the inner Van Allen belt. This was estimated as $\sim 1.08 \times 10^5$ MeV/sec. The photomultiplier tube saturates near 100 μA; thus the maximum current calculated for the peak flux was limited to 20 μA, to provide a factor of 5 for safety. The calibration factor to be derived was then

$$F_{calc} = \frac{1.08 \times 10^5}{20} \frac{\text{MeV}}{\mu\text{A} \cdot \text{sec}} = 5400 \frac{\text{MeV}}{\mu\text{A} \cdot \text{sec}}$$

The calibration procedure was to irradiate the detector with a 1 mCi Cs^{137} source (the crystal is shielded by 5 g/cm^2 aluminum). Only the Cs^{137} gamma and bremsstrahlung would be present inside the shield. A multi-channel analysis was made of the anode pulses from the photomultiplier tube, and the anode current was monitored. The energy calibration per channel was done by identifying the 662 keV Cs^{137} gamma peak (3.28 keV/channel) and calculating the area under the spectrum (1.02×10^8 counts $\times$ number of channels). Therefore the total energy flux seen by the crystal was, for a time of 600 seconds, $E_T = 557.5$ MeV/sec. The anode current measured was 0.102 μA, so that

$$F_{meas} = \frac{E_T}{I_a} = 5483 \text{ MeV}/\mu\text{A} \cdot \text{sec}$$

The run was then taken at a high voltage value of 820 V. If the measured F did not equal the calculated F, the high voltage could be adjusted to yield the correct measured F. This is done by constructing a curve of anode current versus high voltage. The ratio of F_{meas} to F_{calc} determines the I_a required to yield the correct factor, and the high voltage is adjusted to yield this current.

The anode current is converted to a d.c. voltage output by the appropriate electronics.

B. *Satellite System*

The above-described instrumentation was integrated into an OV1-2 Satellite built by General Dynamics Corporation for the Air Force.

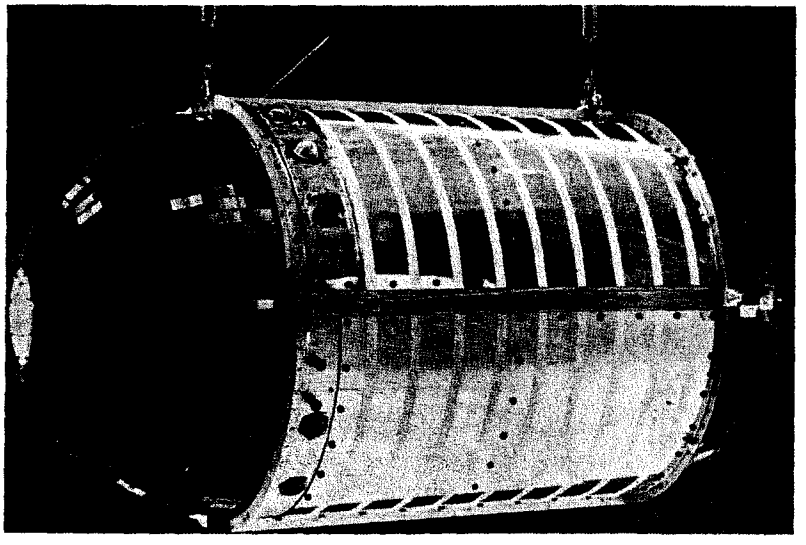

FIG. 2. OV1-2 Satellite (1965 78A)

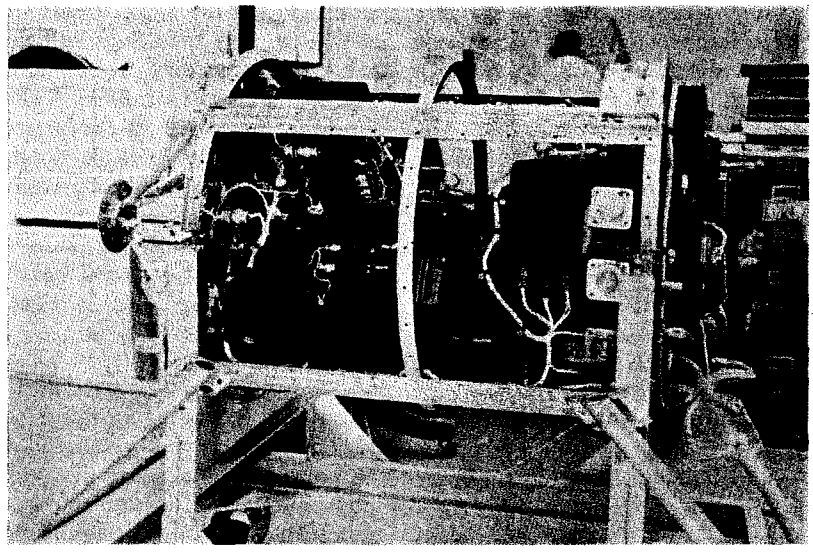

FIG. 3. Layout of instruments.

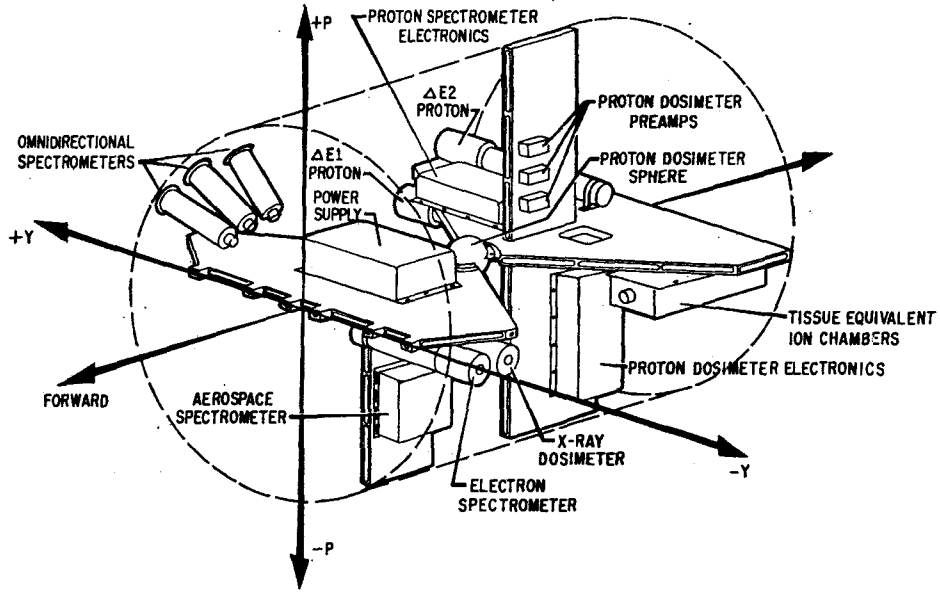

FIG. 4. Layout of instruments (OV1–2).

This satellite is shown in Fig. 2. and the instrument layout is shown in Figs. 3 and 4.

An additional instrument, a three axis magnetometer, was provided as an integral part of the satellite system. This provided information regarding the orientation of satellite axes with respect to the magnetic field line. This allows the measurement of any particle angular distribution which may be present. The ability to independently command each instrument on and off was also provided.

The instrument outputs could be stored on tape for 120 min and read out on command, allowing the accumulation of entire orbits of data. A separate command bypassed the tape recorder and allowed the instruments to be read out in real time.

C. *Spacecraft Material Distribution*

The purpose of the space flight experiment was the correlation of dosimetry and radiation environment measurements; hence, the material distribution surrounding the various dosimeters had to be well known in order to calculate dosimeter response. Even for the simple spherical geometry where the proton dosimeter is located at the geometric center of the spacecraft (Figs. 3 and 4), shielding by other instruments, spacecraft structure, etc., introduce perturbations which must be considered.

Since protons and electrons lose energy mainly through collisions with atomic electrons (to a first order approximation), it will be sufficient to specify the areal density of electrons as a function of solid angle about the point of interest. In general, neither the collision stopping power of primary charged particles or photon attenuation, in the Compton region, is a strong function of attenuator atomic number. It is evident that if the photon attenuation throughout the vehicle geometry is determined the areal electron density may be easily calculated. Aluminum is extensively used in space vehicle construction, and since aluminum is a representative low Z material, the areal density may be expressed in g/cm^2 of aluminum, or the aluminum equivalent electron/cm^2 of path length.

A 1.0 μCi Co^{60} source was positioned at the center of the aluminum sphere (proton dosimeter) in the satellite vehicle. The vehicle could be positioned accurately through three degrees of freedom. A 2 $\times$ 2 in. NaI crystal was located at a distance where it subtended a 1° half-angle from the source. The remainder of the experimental apparatus is shown in Fig. 5. At these (Co^{60}) energies Compton Scattering is the dominant loss mechanism (98%). Thus a measurement of the unscattered to scattered photons yields the areal density through the following relation:

$$I = I_0 e^{-tx}$$

where I = unscattered photons,
I_0 = total photons before absorption,
t = mass absorption coefficient, cm^2/g,
x = absorber path length, g/cm^2.

Using the above technique over 800 solid angles were scanned and translated into equivalent aluminum thickness or areal density.

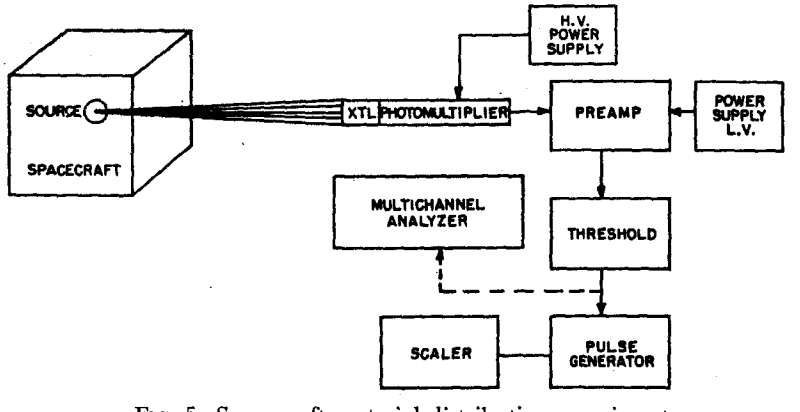

FIG. 5. Spacecraft material distribution experiment.

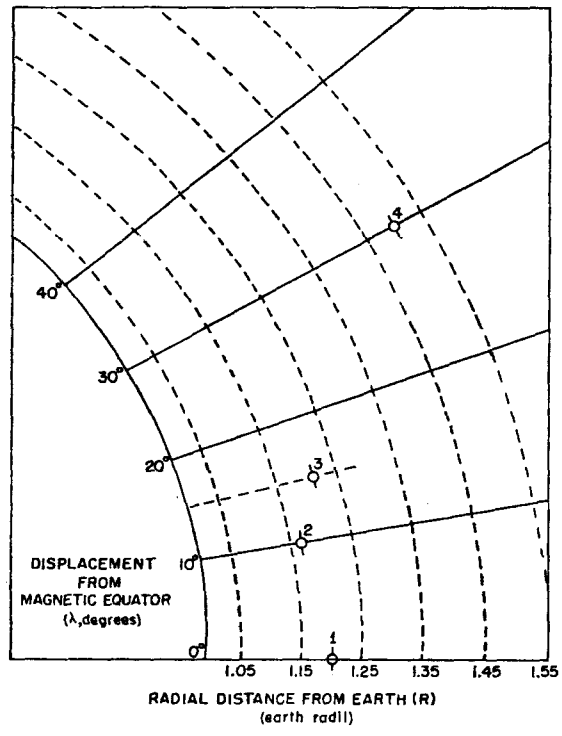

FIG. 6. Spatial location of data points.

A technique was also developed for utilizing this data to specify the material distributions about all dosimeter locations.

III. EXPERIMENTAL RESULTS

This experiment was placed in orbit aboard the OV1-2 Satellite on October 5, 1965. A retrograde orbit with an 1865 n-mi apogee, a perigee of 222 n-mi, and an inclination of 144° were achieved. This orbit was such that nearly all of the Inner Van Allen Zone is swept out by succeeding orbits.

The data reduction has been fully automated and computerized. The instrument calibrations, temperature calibrations, and tape recorder nonlinearities, etc., are removed and the data is printed out as raw count rates, dose rates, etc., as a function of time and spatial position. For convenience in handling, as well as standardization, the spatial position is given in terms of the four parameters R, λ, B, and L. R is the radial geocentric distance to the point, λ is the angular displacement from the magnetic equator, B is the magnetic field strength, and L is the "McIllwain Parameter" [7] which corresponds to the radial, geocentric distance at the equator of the magnetic field line which passes through the point.

Four points in space were arbitrarily selected for this paper. These points are shown in Fig. 6. This figure also depicts the general limits of the satellite coverage. Table 3 gives the pertinent information regarding the selected points.

A. *Electron Spectra*

The outputs of each electron spectrometer channel were plotted as a function of time, and the peak fluxes were selected. These peak fluxes correspond to the instrument aperture being aligned at 90° to the magnetic field line (i.e. at the maxima of the angular distribution). The Greenwich Mean Time of the exact point in space was determined, and the data for a four-minute interval of time around the point was reduced.

Figure 7 shows such data for two spectrometer channels. The modulation is caused as

Table 3. Points Selected for Analysis

Point	R (Earth radii)	B (gauss)	L (Earth radii)	λ (degrees)	Date/Orbit
1	1.20	0.178	1.20	0	9 Oct/29 14 Oct/100
2	1.17	0.200	1.20	9.5	12 Oct/75
3	1.23	0.199	1.30	16	9 Oct/42
4	1.51	0.120	2.00	30	6 Oct/10

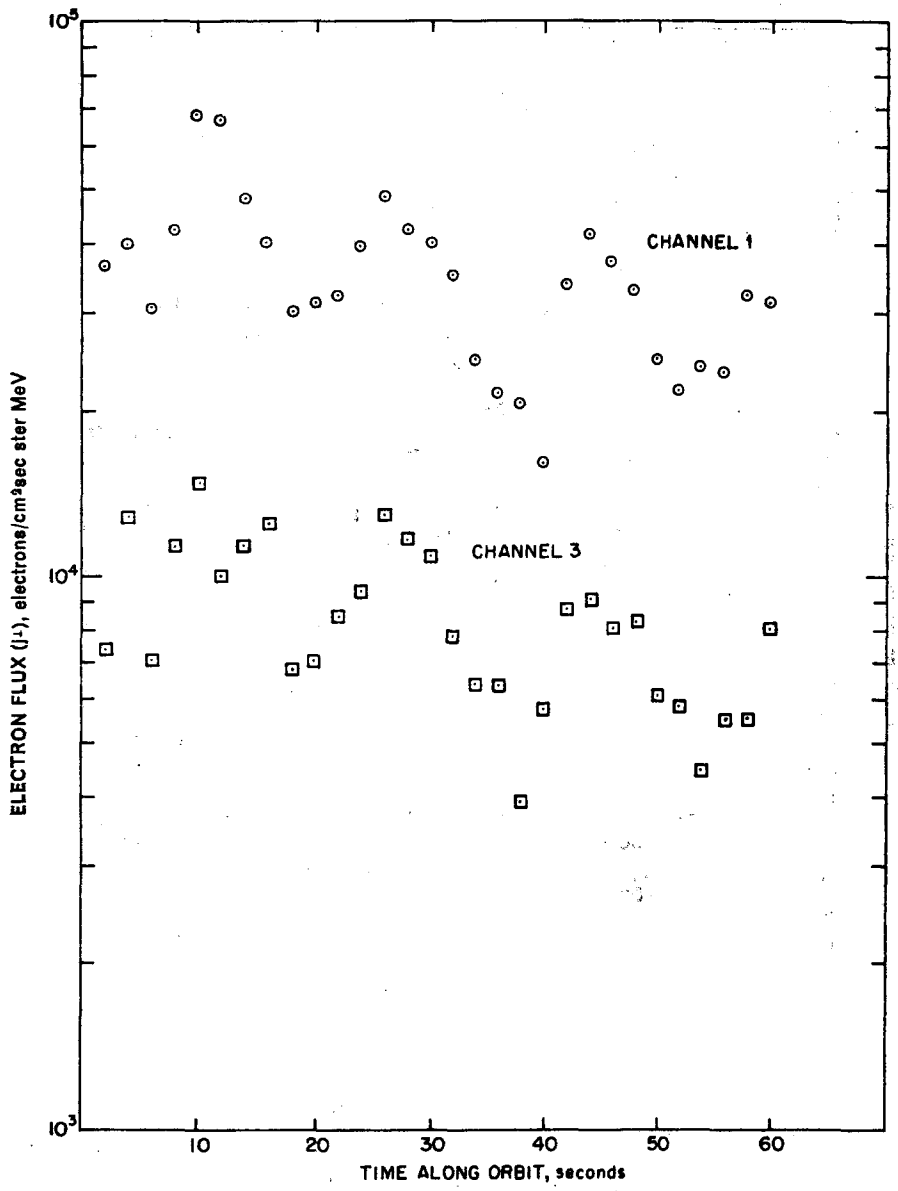

FIG. 7. Electron spectrometer channels 1 and 3, $L = 1.20$, $\lambda = 0°$.

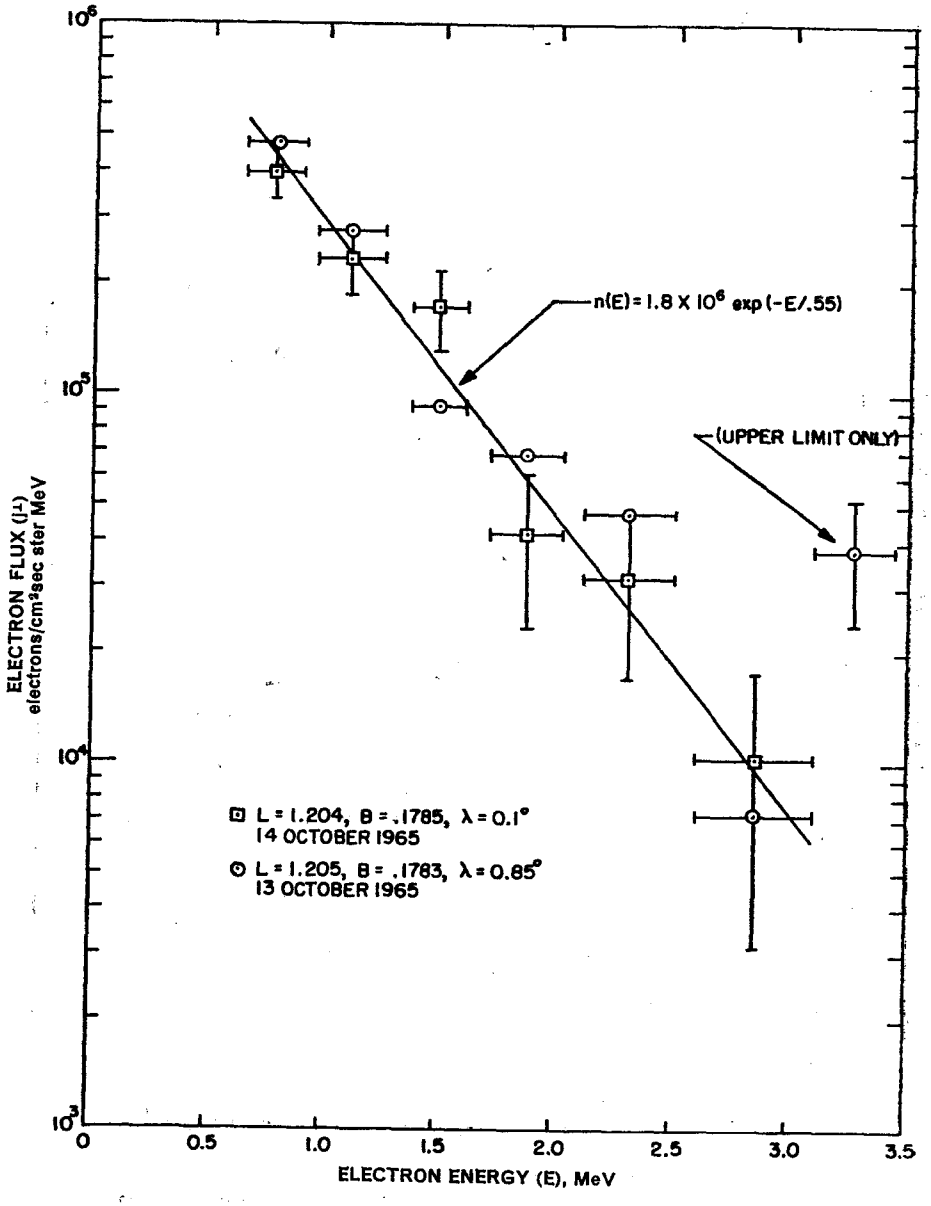

FIG. 8. Differential electron spectrum, October 13–14, 1965.

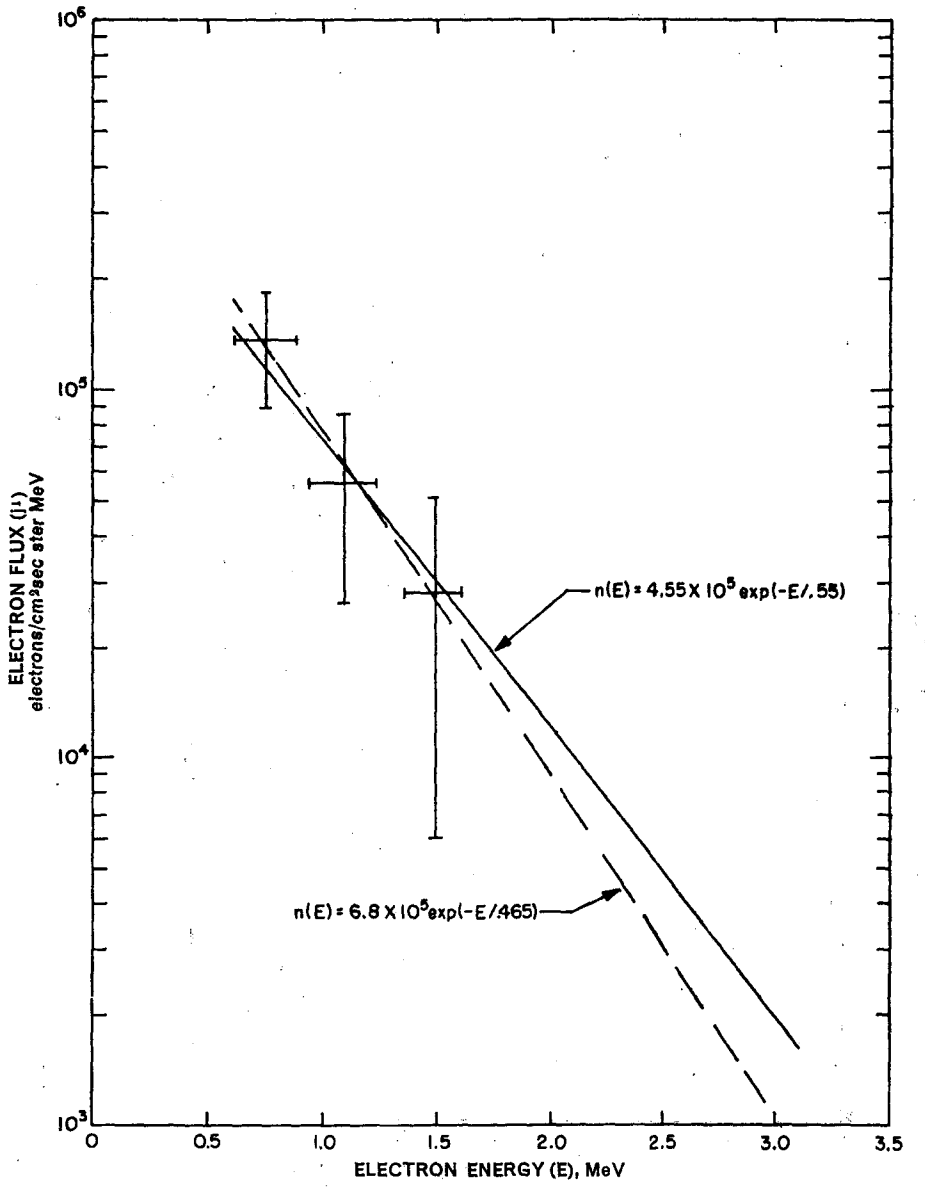

FIG. 9. Differential electron spectrum, October 12, 1965, $L = 1.207$, $B = 0.200$, $\lambda = 9.46°$.

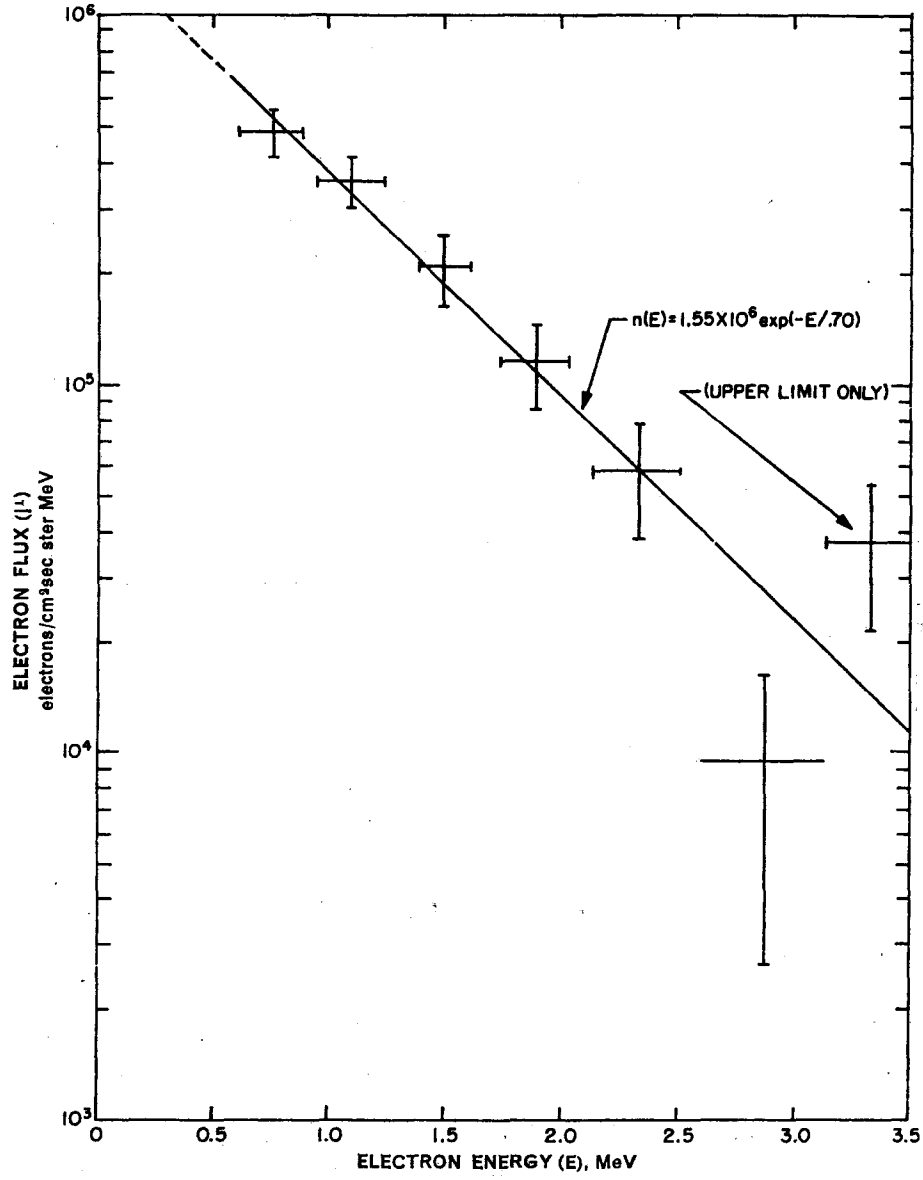

FIG. 10. Differential electron spectrum, October 9, 1965, $L = 1.30$, $B = 0.1993$, $\lambda = 16°$.

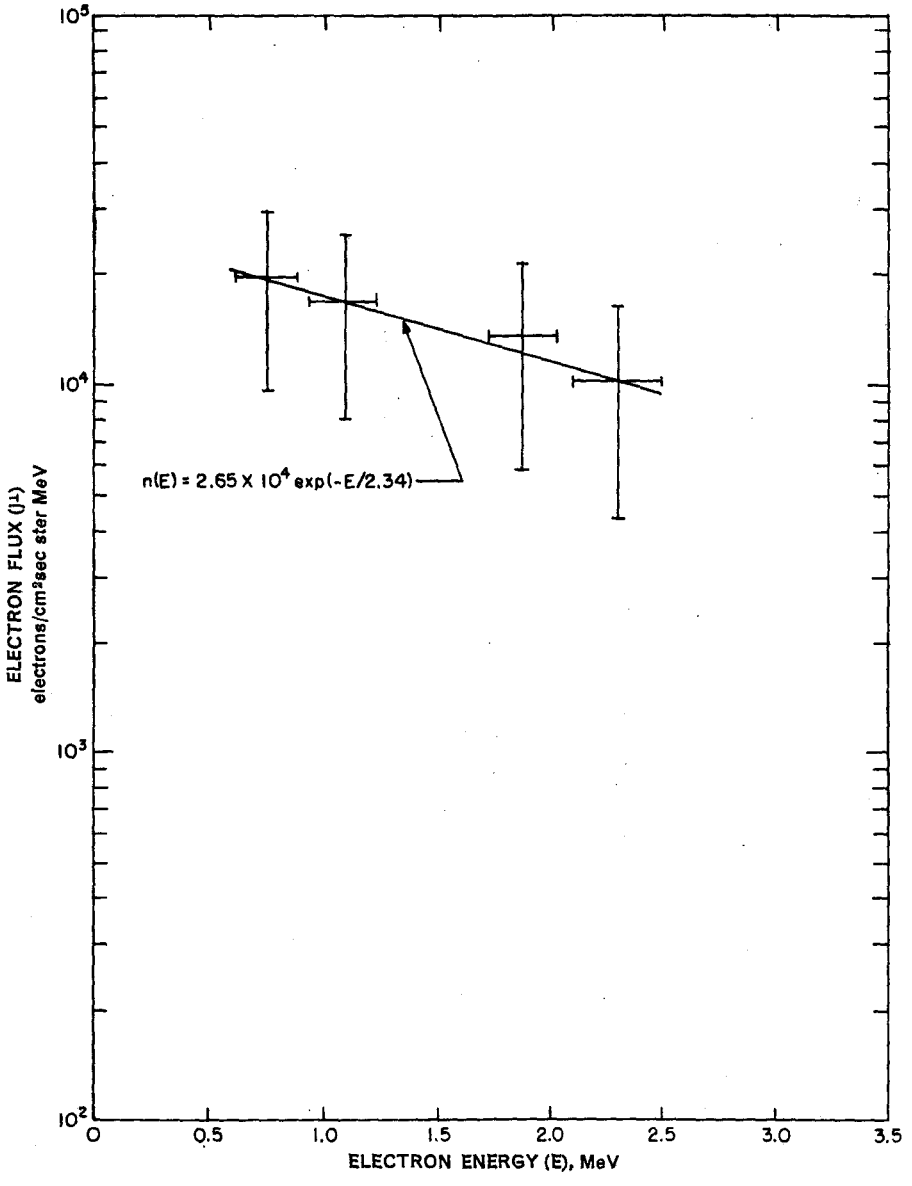

FIG. 11. Differential electron spectrum, October 6, 1965, $L = 2.00$, $B = 0.120$, $\lambda = 29.8°$.

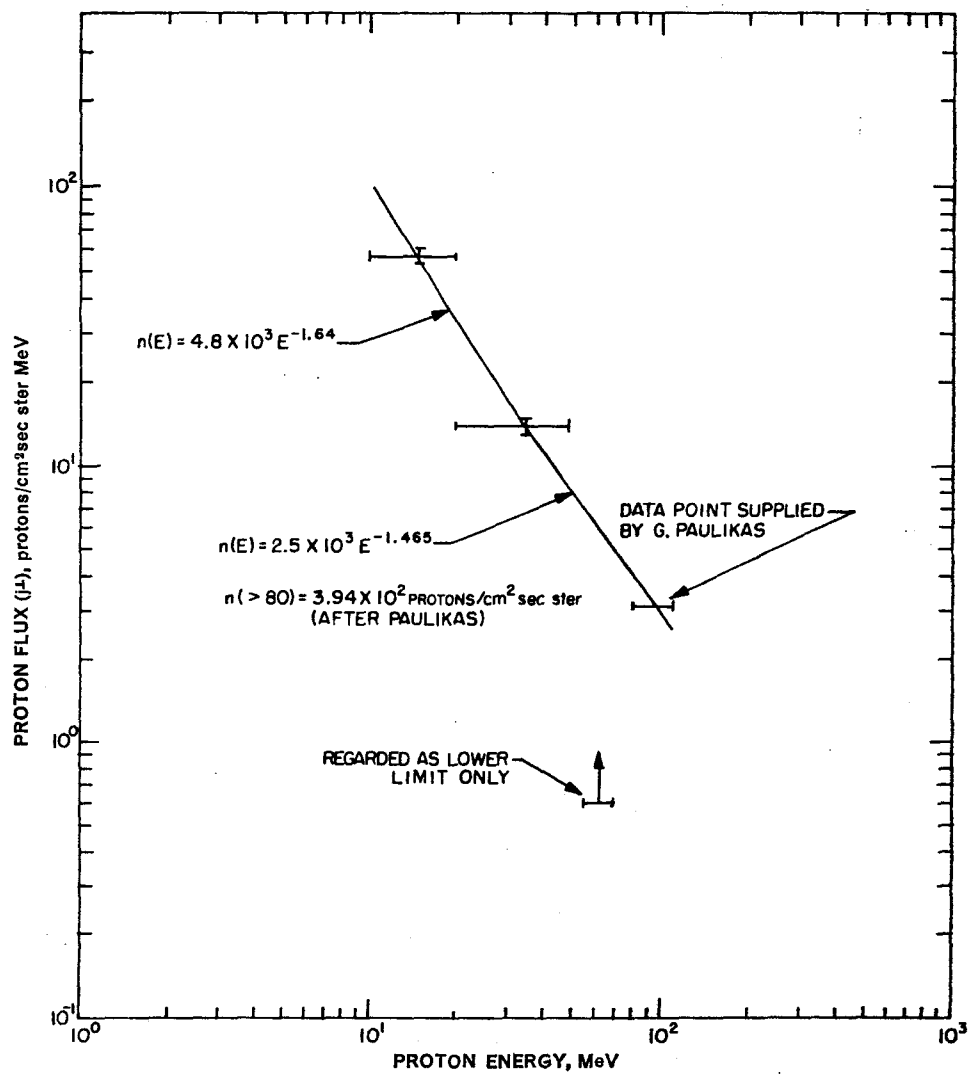

FIG. 12. Differential proton spectrum, October 1965, $L = 1.20$, $B = 0.178$, $\lambda = 0°$.

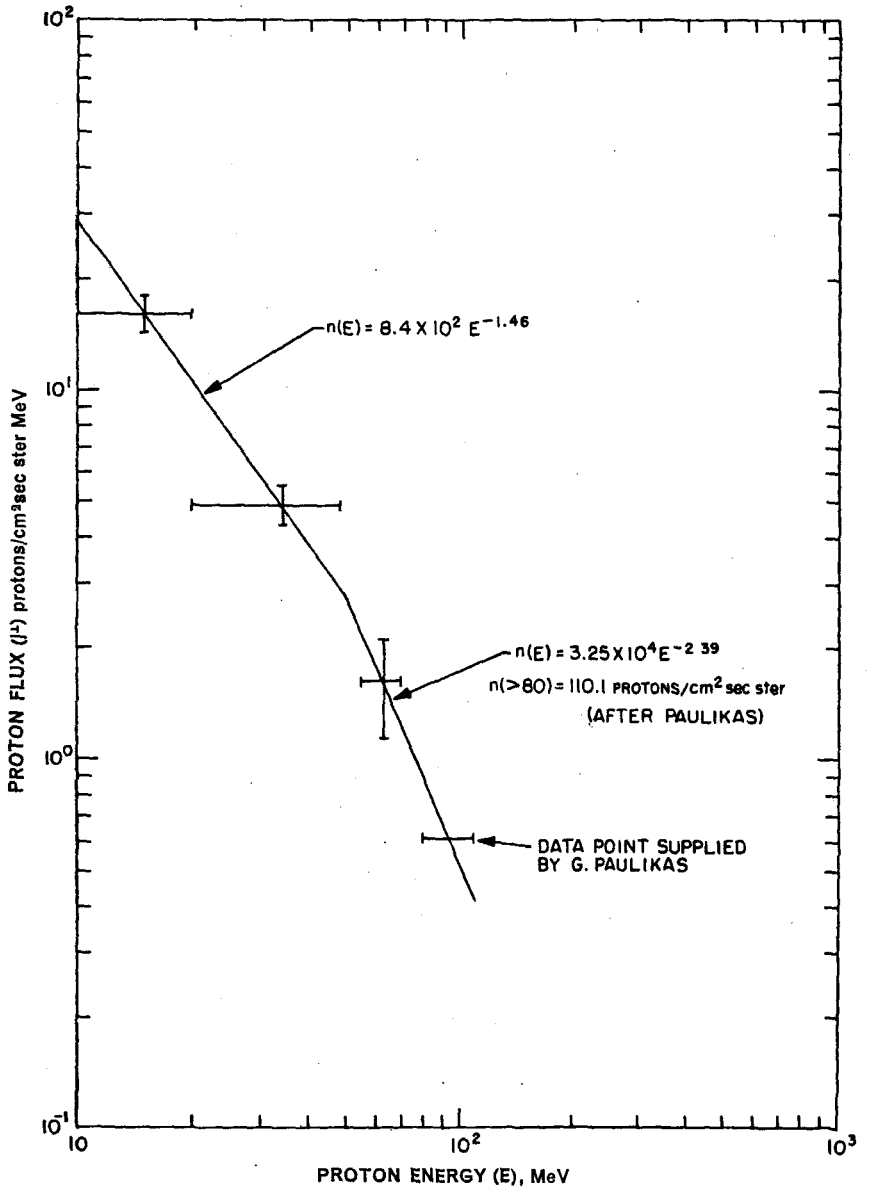

FIG. 13. Differential proton spectrum, October 12, 1965, $L = 1.207$, $B = 0.200$, $\lambda = 9.46°$.

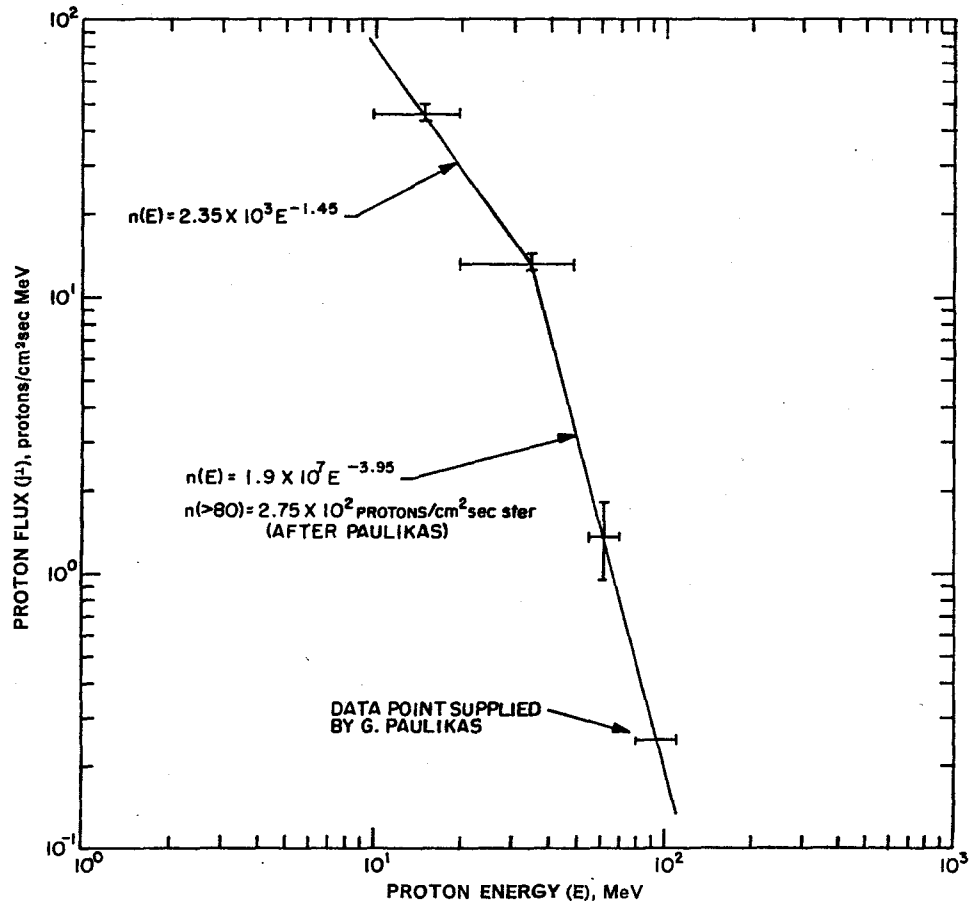

FIG. 14. Differential proton spectrum, October 9, 1965, $L = 1.30$, $B = 0.1993$, $\lambda = 16°$.

the vehicle tumbles in space and the directional aperture passes in and out of the plane of maximum intensity. This modulation is typical for all directional instruments.

Figures 8, 9, 10, and 11 show the spectra determined for each of the four points. Following earlier experimenters, the data have been fitted with analytical expressions of the form $N(E) = A \exp(-E/E_0)$. These expressions as found for the four points are as follows:

Point 1: $N(E) = 1.8 \times 10^6 \exp(-E/0.55)$

Point 2: $N(E) = 6.8 \times 10^5 \exp(-E/0.46)$ or $4.55 \times 10^5 \exp(-E/0.55)$

Point 3: $N(E) = 1.55 \times 10^6 \exp(-E/0.70)$

Point 4: $N(E) = 2.65 \times 10^4 \exp(-E/2.34)$

There has been postulation by many experimenters, with some verification, that the electron spectral slope does not change with B (or λ) along points of constant L. It should be observed that while the best fits are not identical, both points 1 and 2 ($L = 1.20$) may be fitted with the same analytical expression within experimental error. The difference in spectral shape and/or flux with other spatial positions should be noted.

B. *Proton Spectra*

To construct proton spectra the data from the two Delta E Spectrometers, the Proton Spectrometer, and one of the Aerospace Omnidirectional Spectrometers ($80 < E < 110$ MeV) [8] were used. The data from the Proton

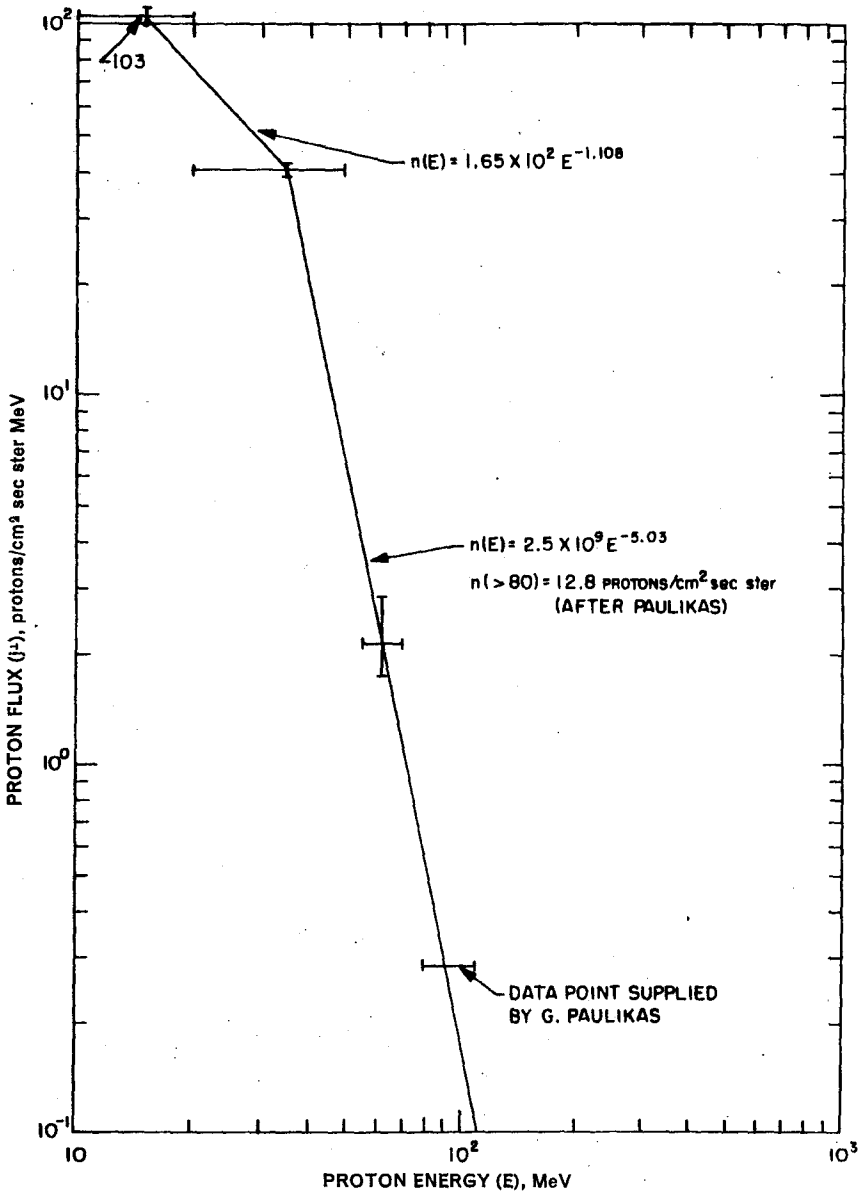

FIG. 15. Differential proton spectrum, October 6, 1965, $L = 2.00$, $B = 0.12$, $\lambda = 29.8°$.

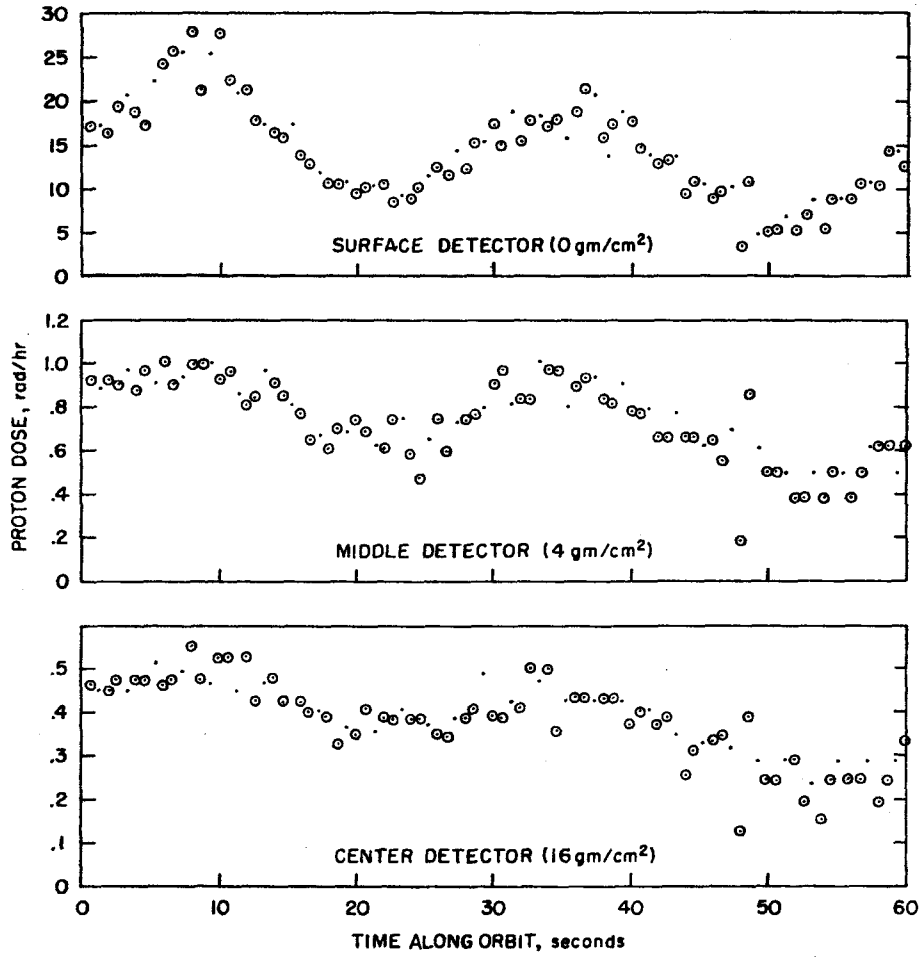

FIG. 16. Proton dosimeter data-revolution 10, October 6, 1965.

Spectrometer was sometimes difficult to interpret due to saturation and at these points the data were considered as lower units only. The data furnished by Aerospace described the omni-directional flux whereas our spectra are in terms of uni-directional fluxes. To convert omni-directional fluxes to uni-directional fluxes a program developed by Dr. Thomas Farley of UCLA was used. The spectrums thus derived are shown in the Figs. 12, 13, 14, and 15. Again following the lead of earlier experimenters, the spectrums were fitted with two power law analytical expressions, of the form $N(E) = AE^{-\gamma}$ over separate energy ranges. These are given for the four points as follows:

Point 1: $N(E) = 4.8 \times 10^3 E^{-1.64}$ $10 < E < 35$ MeV

$N(E) = 2.5 \times 10^3 E^{-1.46}$ $35 < E < 110$ MeV

Point 2: $N(E) = 8.4 \times 10^2 E^{-1.46}$ $10 < E < 50$ MeV

$N(E) = 3.25 \times 10^4 E^{-2.30}$ $50 < E < 110$ MeV

Point 3: $N(E) = 2.35 \times 10^3 E^{-1.45}$ $10 < E < 35$ MeV

$N(E) = 1.9 \times 10^7 E^{-3.95}$ $35 < E < 110$ MeV

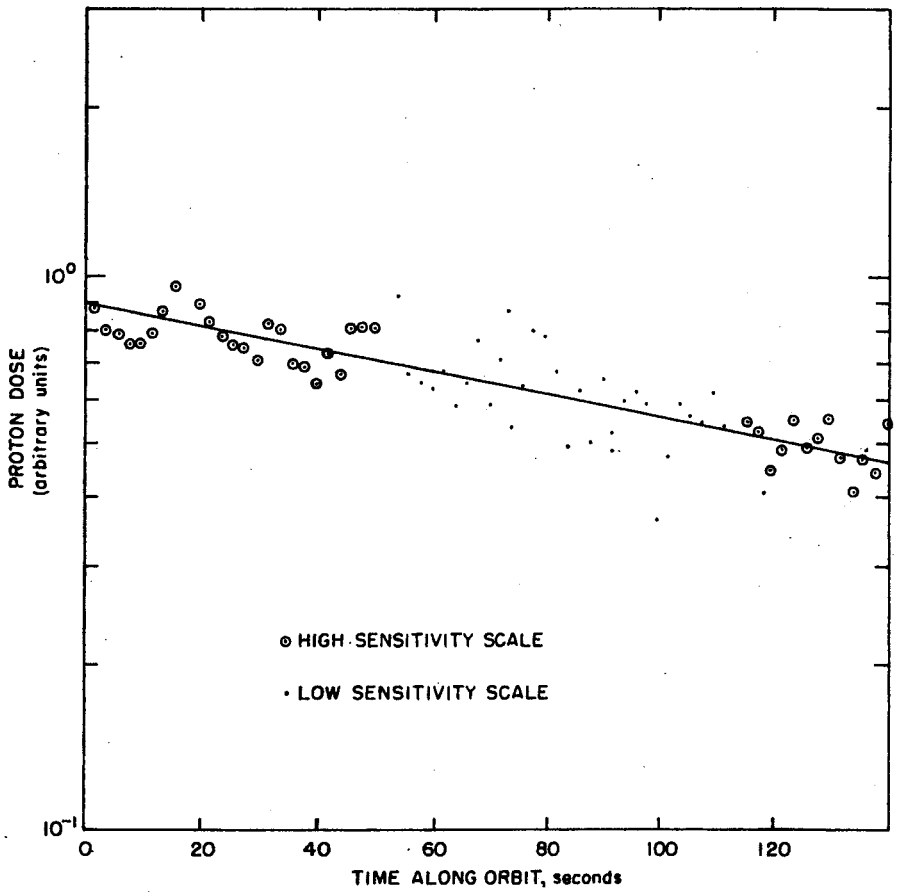

FIG. 17. Proton dosimeter middle detector, method of dose determination.

Point 4: $N(E) = 1.65 \times 10^{2} E^{-1.74}$ $10 < E < 35$ MeV

$N(E) = 2.5 \times 10^{9} E^{-5.03}$ $35 < E < 110$ MeV

As with the electron spectrums, the change in flux intensity and spectral shape with spatial position should be noted.

C. *Dose Rate Measurements*

The experimental radiation dose rates at the four chosen positions in space were obtained for the same time that the spectral determinations were made. Six experimental doses were obtained at each point in space from: three solid-state proton dosimeters, one X-ray detector, and two tissue-equivalent ionization chambers. The radiation dose rate determinations, the general dose rate variation with time, and the experimental dose rate variation are discussed for the various instruments in the following paragraphs.

1. Proton Dosimeters. The proton dosimeters are sampled every two-thirds of a second. A typical output for 1 min is illustrated in Fig. 16. This shows the roll-modulated output, the range switching, and the general fluctuation in the experimental data. The dose rate for the desired time, corresponding to the desired point, was determined by plotting the average of three dose rates for two plus minutes and then drawing a line through the data. (An example of this technique is shown in Fig. 17) The proton dosimeter changes scale approximately every

Table 4. Proton Dosimeter Doses for the Four Selected Locations in Space

Detector	Point in space	Dose rate (rad/hr)	Rate of change (rad/hr/min)	% Variation	
				Positive	Negative
Surface (0 g/cm²)	1	6.9	5.5	41	41
	2	1.7	2.1	37	41
	3	9.4	1.0	35	25
	4	2.8	0.47	26	48
Middle (4 g/cm²)	1	0.64	0.19	33	35
	2	0.21	0.11	22	18
	3	0.46	0.08	22	18
	4	0.066	0.014	71	29
Center (16 g/cm²)	1	0.49	0.12	32	22
	2	0.16	0.08	39	32
	3	0.34	0.06	20	13
	4	0.15*	—	—	—

* Indicates an upper limit only.

Table 5. X-ray Detector Doses for the Four Selected Locations

Point in space	Dose rate (rad/hr)	Rate of change (rad/hr/min)	% Variation	
			Positive	Negative
1	0.80	0.26	10	10
2	0.25	0.11	26	22
3	0.50	0.08	23	14
4	0.099	0.03	35	23

Table 6. T.E.I.C. Doses for the Four Locations

Point in space	Dose rate—T.E.I.C. No. 1 (rad/hr)			Dose rate—T.E.I.C. No. 2 (rad/hr)		
	Peak	Minimum	Average	Peak	Minimum	Average
1	4.8 ± 0.9	2.1 ± 0.5	3.6 ± 0.8	3.0 ± 1.0	3.6 ± 0.6	4.2 ± 0.8
2	1.6 ± 0.6	0.7 ± 0.2	1.2 ± 0.3	1.5 ± 0.3	1.2 ± 0.3	1.4 ± 0.3
3	6.6 ± 1.2	1.9 ± 0.6	4.7 ± 0.6	3.6 ± 0.6	2.5 ± 0.5	3.1 ± 0.5
4	0.7 ± 0.3	0.3 ± 0.1	0.5 ± 0.2			0.3 ± 0.1

minute and may be "off-scale" for one minute but may be providing good data both before and after that minute. Plotting more than 2 min centered about the off-scale data provides useful dose rate versus time information. The dose rate is then determined at the desired time (point), the time variation is determined, and the percentage variation (roll modulation) of dose rate is noted.

The results for the proton dosimeters are listed in Table 4. The center (16 g/cm^2) dosimeter was always below its minimum sensitivity at $L = 2.0$, $B = 0.122$ and only an upper limit of 0.015 rad/hr could be determined.

2. X-Ray Detector. The X-ray detector was sampled once every two seconds. This data was plotted against time. As with the proton dosimeter data, a line was drawn through the data. The dose rate was then determined at the desired time, the time variation determined, and the experimental variation noted. Results for the four positions are tabulated in Table 5.

3. Tissue-equivalent Ionization Chambers (T.E.I.C.). The data from the two tissue-equivalent ionization chambers were reduced in a manner similar to that from the other dose rate instruments except that the peak rates as well as an average over a roll modulation were determined. This was done in an effort to further evaluate the effect of the material distribution of the satellite. The results are shown in Table 6. T.E.I.C. No. 1 is shielded by 0.17 g/cm^2 and T.E.I.C. No. 2 by 3.2 g/cm^2.

IV. COMPARISON OF EXPERIMENTAL AND CALCULATED RESULTS

In the previous sections, an experiment has been described the results of which may be used to assess the validity of certain assumptions basic to computer programs used in predicting dose rates which may be encountered in space. In addition, the strengths and weaknesses of many of the sub-routines, such as radiation transport and dose conversions, may be determined.

Preliminary dose calculations have been performed, for certain cases, to provide a general comparison of calculated and experimental dose at three of the points discussed in the previous sections. These calculations have been performed only for two detectors of the Proton Spectrometer (0.0 g/cm^2 and 4.0 g/cm^2) and the most thinly shielded ionization chamber (0.17 g/cm^2).

For the case of the ionization chambers two of the available computer programs (Boeing[2]

Table 7. Comparison of T.E.I.C. No. 1 Dose Rate Calculations to Measurements

Point in space	Type of dose rate*	Dose rates in rad/hr	
		AFWL-Boeing	AMRL-Northrop
1	Electron	3.2	3.6
	Proton	1.6	2.8
	Total	4.8	6.4
	Expt.	3.6 ± 0.8	3.6 ± 0.8
2	Electron	1.4	0.8
	Proton	0.8	0.3
	Total	2.2	1.1
	Expt.	1.2 ± 0.3	1.2 ± 0.3
3	Electron	3.2	7.9
	Proton	0.8	1.6
	Total	4.0	9.5
	Expt.	4.7 ± 0.9	4.7 ± 0.9

* The photon dose rate was negligible in all cases when compared to primary dose rate.

Table 8. Comparison of Proton Dosimeter Dose Rate Calculations to Measurements (AMRL-Northrop method only)

Point in space	Type of dose rate	Dose rates in rad/hr	
		Surface detector (0 g/cm²)	Middle detector (4 g/cm²)
1	Electron	4.6	–0–
	Proton	3.2	0.4
	Total	7.8	0.4
	Expt.	6.9	0.6
2	Electron	1.1	–0–
	Proton	0.3	0.1
	Total	1.4	0.1
	Expt.	1.7	0.2
3	Electron	9.6	–0–
	Proton	2.0	0.03
	Total	11.6	0.03
	Expt.	9.4	0.46

and Northrop[3]) were utilized in making calculations. Only the Northrop program was utilized in calculations concerning the Proton Spectrometer.

The results of the above calculations and comparisons with the experimental data are presented in Tables 7 and 8. These data should be viewed as preliminary serving only as an example of the results which may be expected from such a technique. No effort was expended to improve or modify the existing calculational procedures other than to further simplify the computational methods.

For a detailed discussion of the calculational methods involved, the reader is referred to refs. 2 and 3.

Three components of the dose were calculated utilizing the particle spectrum obtained by this experiment at the spatial locations involved. These were: (1) dose due to primary protons; (2) dose due directly to electrons; and (3) dose due to photons produced by the slowing down of electrons. Each dose component has assumptions peculiar to the calculations which yield the dose rate for primary particles versus the material thickness for that dose component. The material thickness about the dose points was calculated from the results of the gamma mapping experiment. The material distribution was obtained directly for the Proton dosimeter sphere and approximated for the ionization chambers assuming a right circular geometry for the satellite experimental bay. Once calculated, each material distribution was grouped according to thicknesses to determine the amount of solid angle having the specified ranges of thickness. For each dose point, this was then plotted as a histogram of solid angle per thickness versus thickness and a smooth curve plotted. The dose rates for proton, electron and photon dose components were then calculated by integrating the product of dose rate and material distribution range. In one case (Northrop), the measured spectra were extrapolated beyond the experimental values (using the shape factors present) before they were input to the calculations. In the second case (Boeing) no such extrapolations were made.

In general, fair agreement was obtained (in spite of the simplifications) at points of thin external shielding. This agreement progressively worsened as the shielding thickness increased; however, the discrepancies may be explained to a large degree by the manner in which the material distribution was handled and to a lesser degree by the spectral extrapolations.

In summary, the radiation transport and dose-conversion portions of the computer techniques seen are verified with the environmental and material distribution inputs being the most critically sensitive. In fact, a separate study of the importance of material heterogeneity in the calculation of radiation doses has shown that the dose rate is underestimated when constant mean thicknesses are used for solid angles which don't really have constant thicknesses. The calculated dose rate can vary a factor of four or more depending on the spectrum, the material thickness, and the degree of heterogeneity, if one first assumes a constant thickness and then takes into account heterogeneities.

REFERENCES

1. W. H. LANGHAM *et al. Aerospace Med.* **36,** Sec. 11. Special Report (Ed. by Langham), Feb. 1965.
2. Air Force Weapons Laboratory. Technical Documentary Report Number WL-TDR-64-71. *Computer Codes for Space Radiation Environment and Shields,* Vol. I, Aug. 1964.
3. R. E. FORTNEY. USAF Aeromedical Research Laboratory Technical Documentary Report Number AMRL-TDR-64-11, *Computer Analysis of Radiation Shielding,* Feb. 1964.
4. S. C. FREDEN and G. A. PAULIKAS. *J. Geophys. Res.* **69,** 1259–1269 (1964).
5. B. C. CLARK. *Life Sciences and Space Research* III (Ed. by M. Flarkin), 29–47. North Holland Pub. Co., 1965.
6. M. C. SCHNEIDER. Air Force Weapons Laboratory. Technical Documentary Report Number WL-TDR-64-96, *Advanced Spaceborne Dosimetry Instrumentation,* Dec. 1965.
7. C. E. MCILLWAIN. *J. Geophys. Res.* **66,** 3681–3691 (1961).
8. G. A. PAULIKAS. Private communication, July 1966.
9. T. A. FARLEY. Private communication, Feb. 1966.